Locomotion Control of Ledge Climbing Robot Using CPG Control and Infrared Sensors

Chi-Ying Lin, *Member, RST,* and Ting-Chun Hu

***Abstract*— Climbing along the horizontal ledges on the vertical walls is insufficient for ledge climbing robots because ledges with non-zero pitch or inclined angles are also highly representative application scenarios. To improve the ability to adapt to the various climbing environments, this study presents a locomotion control strategy composed of a central pattern generator based algorithm to perform horizontal ledge climbing and a path planning algorithm to pass through the non-smooth inclined transition. Two sets of infrared sensors are installed on both sides of the robot to acquire environment information and develop an algorithm that detects and estimates the pitch angle change while the robot is transversely climbing along pitched ledges. A gripper posture feedback control system is integrated into the process of horizontal ledge climbing to enhance the robustness against disturbances. Experiments mimicking the ledge climbing scenarios with both negative and positive pitch angles are conducted to justify the effectiveness of the proposed locomotion control strategy.**

Keywords—climbing robot, pitched ledge climbing, locomotion control

I. INTRODUCTION

Wall climbing robots have been widely developed to facilitate tasks such as surveillance, reconnaissance, rescue, inspection and maintenance. Among the existing climbing robots, ledge climbing robot is a specialized robot designed to move along the ledges on the exterior walls by alternating its two hands to grab the ledges and move forward. This locomotion style is motivated by the continuous motion of the video clips from human ledge climbers and could be simplified as the movement of human upper body for easier robot implementation [1]. The most apparent difference between ledge climbing robots and other existing climbing robots includes two parts: (1) The ledge climbing robots use two arms to perform climbing motion and could be also categorized as biped climbing robots [2-4] or brachiating robots [5-9] showing better agility; (2) The ledge climbing robots make good use of the ledges on the exterior walls to perform climbing locomotion, but most climbing robots [10], on the contrary, treat these ledges as obstacles instead and usually suffer from the burden of developing complex obstacle avoidance algorithms together with bulky robot mechanisms [11-13].

Because roofed houses belong to the fundamental elements in today's domestic architecture, to initiate a generalized investigation this study classifies the application scenarios suitable for ledge climbing robots into three simple types based on the value of roof pitch angles (or inclined angles): horizontal or flat ledges, double pitched ledges, single pitched ledges. Fig. 1 illustrates these three classifications corresponding to the flat roof, the double pitched roof, and the single pitched roof commonly existed in the residential buildings [14]. As can be seen, the horizontal ledges have zero pitch angles where the double pitched ledges have negative pitch angles and single pitched roofs have positive pitch angles. The ledges with varying inclined angles could also be easily found in similar structures such as windowsills or eaves for the purpose of drainage design.

To realize the locomotion of horizontal ledge climbing in Fig. 1(a) the authors in [1] have designed a central pattern generator (CPG) based locomotion controller which applies five oscillators [15,16] to generate robot joint commands for synchronized and periodic like transverse ledge climbing movement. The phase coupling parameters in the oscillators were found through an optimization process such that the robot can perform the ledge climbing locomotion of human athletes solely using upper body. The experimental results showed that the robot not only can perform both right ledge climbing and left ledge climbing tasks but also can smoothly switch between these two locomotion styles during gait transition, greatly reducing the risk of making robot falling on the ground.

Although the CPG controller applied in [1] seems to be working very well for continuous horizontal ledge climbing, obviously this locomotion control strategy is still not applicable to the application scenarios shown in Fig. 1(b) & (c) because of lack of ability to detect the existence of ledge inclination and pass through the turning point under robot mechanism constraints. To solve this problem and broaden the application range of ledge climbing robots, this study proposes a locomotion control strategy which integrates the use of infrared sensors with CPG algorithm to simultaneously handle the tasks of horizontal and pitched ledge climbing. After analyzing two possible robot gaits, a multi-step crossing gait is chosen to overcome the inclined transition in which the maximum pitch angle is limited by robot kinematic constraints. Because of the opposite sign between double pitched (negative) and single pitched (positive) ledges, the algorithm of detecting and estimating the pitch angle is developed by placing two infrared sensors at each side of robot arm for the cases of looking down and looking up, respectively. Starting with CPG algorithm for horizontal ledge climbing, the proposed locomotion control strategy switches to the path planning mode when detecting a ledge inclination change. After passing through the turning point the robot then immediately switches back to CPG algorithm for continuous ledge climbing. Experiments of climbing double pitched and single pitched ledges are finally

This work was supported by the Ministry of Science and Technology, Taiwan, under grant MOST-108-2628-E-011-004.

C.-Y. Lin is with the is with the Mechanical Engineering Department, National Taiwan University of Science and Technology, Taipei 106, Taiwan. (e-mail: chiying@mail.ntust.edu.tw)

T.-C. Hu, was with National Taiwan University of Science and Technology, Taipei 106, Taiwan. (e-mail: azsxdc118319@gmail.com).

presented to demonstrate the effectiveness of the proposed locomotion control strategy.

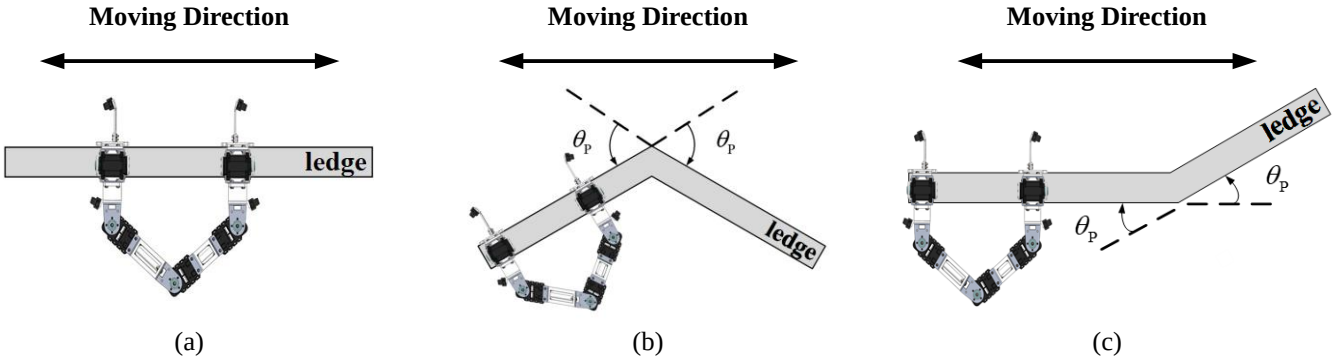

(a) (b) (c)

Fig. 1. Application scenarios for ledge climbing: (a) horizontal (flat) ledge; (b) double pitched ledge; (c) single pitched ledge. θ_p is the pitched angle w.r.t. moving direction, where $\theta_p < 0$ in case (b) and $\theta_p > 0$ in case (c).

II. Ledge Climbing Robot

This section first presents the system hardware and specs of the applied ledge climbing robot. Two possible gaits while climbing pitched ledges are then analyzed to identify the used gait and maximum ledge slope the robot can handle with in this study. The placement of infrared sensors along with the relationship between ledge slope and sensor measured values are also provided to develop the locomotion control strategy which will be discussed in the next section.

A. System Description

As shown in Fig. 2, the robot developed in our previous work [1] refers to the ledge climbing locomotion of human athletes as a 5 DOF mechanism, including joints *Gl, Gr, Al, Am,* and *Ar*. Among these joints, the former two joints *Gl* and *Gr* represent the joints which can open and close the grippers, in which the later three ones represent the left-middle-right joints between shoulder and arm. Servo motors are installed with the robot joints to realize locomotion control. The whole length of the robot is close to 400 mm and the maximum climbing distance for each locomotion cycle is roughly 100 mm.

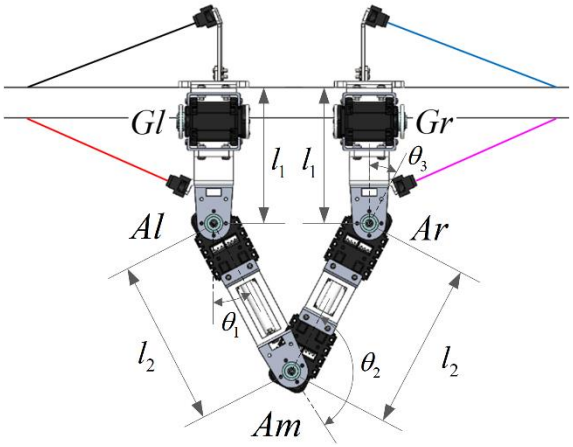

Fig. 2. Schematic diagram of the developed ledge climbing robot. Infrared sensors are placed at the top of the upper claw and the side of the robot arm to detect the location of the target ledge.

This research considers the problem of continuous ledge climbing subject to unknown ledge slope changes. Infrared sensors [17] are used to detect any possible ledge slope variation while the robot moves. There are two kinds of slope detection results, while positive and negative slope values indicate the cases of increasing and decreasing the heights of the robot climbing along the ledge, respectively. In particular, two pairs of infrared sensors (GP2Y0A41SK0, SHARP) are attached to the top of the upper claws and to the side of the robot arms to identify the next targeted ledge location that the robot should grab in each locomotion cycle. The measured IR sensor errors after signal processing are within the range of ±1 mm.

1) Robot gait Analysis while climbing along the pitched ledge

Climbing along the pitched ledge requires that the robot autonomously adjusts its gait to overcome the abrupt ledge slope changes without falling on the ground. The gaits that can deal with the slope turning point based on the designed robot are classified as one-stride crossing and multi-step crossing, as shown in Fig. 3. Although the gait of one-stride crossing seems to be more efficient than using the gait of multi-step crossing, it is also very difficult to realize this gait because of the more strict mechanism constraints imposed by the ledge slope. Therefore, this study adopts the gait of multi-step crossing to perform non-horizontal ledge climbing. To find the maximum slope values of the ledge the robot can climb, assume the robot posture satisfies the case of two grippers closest to each other under mechanical constraints with one hand fixed.

Fig. 4 represents the end-effector position of the grasping gripper $Q(x,y)$ when the robot moves right to start the first step of multi-step crossing with a pitched angle β. In this figure, R_{min} is the minimum distance between two hands, g_w is the half distance of the gripper width, and l_1 and l_2 are the lengths of the robot elbow and arm, respectively. Using the world coordinate (X,Y) shown in Fig. 4, one can represent the coordinate of the target grasping position $Q(x,y)$ as

$$\begin{cases} x = -l_1 - g_w \sin\beta \\ y = R_{\min} + g_w + g_w \cos\beta = R + g_w \cos\beta \end{cases} \quad (1)$$

where $R = R_{min} + g_w$. The solution of this three-link articulated robotic manipulator exists only if the kinematic constraint of second joint angle satisfies the trigonometric inequality expressed below:

$$\left| \frac{\left((-l_1 - g_w \sin\beta) + l_1 \cos\beta\right)^2 + \left(\left(R + g_w \cos\beta\right) + l_1 \sin\beta\right)^2 - l_2^{\,2} - l_2^{\,2}}{2 l_2 l_2} \right| \le 1$$

$$\Rightarrow \left(-l_1 - g_w \sin\beta + l_1 \cos\beta\right)^2 + \left(R + g_w \cos\beta + l_1 \sin\beta\right)^2 - l_2^{\,2} - l_2^{\,2} \le 2 l_2^{\,2}$$

(2)

Let $\sin\beta = \frac{2t}{1+t^2}$, $\cos\beta = \frac{1-t^2}{1+t^2}$, $t = \tan\frac{\beta}{2}$ and reorganize the above equation. The transformed one-variable inequality now can be represented as

$$t^2\left(4l_1^{\,2} + g_w^{\,2} + R^2 - 4l_2^{\,2} - 2g_wR\right) + t\left(4l_1g_w + 4l_1R\right) + \ldots \\ 2g_wR + g_w^{\,2} + R^2 - 4l_2^{\,2} \le 0 \tag{3}$$

Solving this inequality and substituting the original variable β back gives the range of the pitched angle without violating the robot kinematic constraints, which can derived as follows

$$\begin{cases} A = 4l_1^{\,2} + g_w^{\,2} + R^2 - 4l_2^{\,2} - 2g_wR \\ B = 4l_1g_w + 4l_1R \\ C = 2g_wR + g_w^{\,2} + R^2 - 4l_2^{\,2} \end{cases} \\ \Rightarrow t_- = \frac{-B - \sqrt{B^2 - 4AC}}{2A} \le t \le \frac{-B + \sqrt{B^2 - 4AC}}{2A} = t_+ \tag{4}$$

$$\cos^{-1}\left(\frac{1-t_-^{\,2}}{1+t_-^{\,2}}\right) \le \beta \le \cos^{-1}\left(\frac{1-t_+^{\,2}}{1+t_+^{\,2}}\right) \tag{5}$$

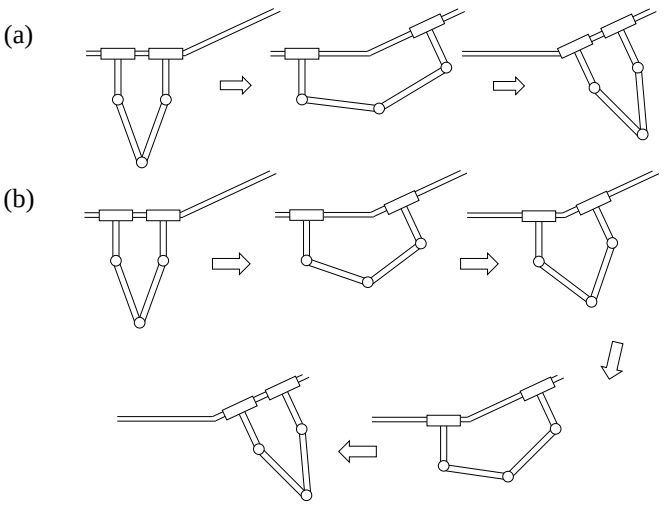

Fig. 3. Possible robot gaits to overcome the ledge slope changes: (a) one-stride crossing; (b) multi-step crossing.

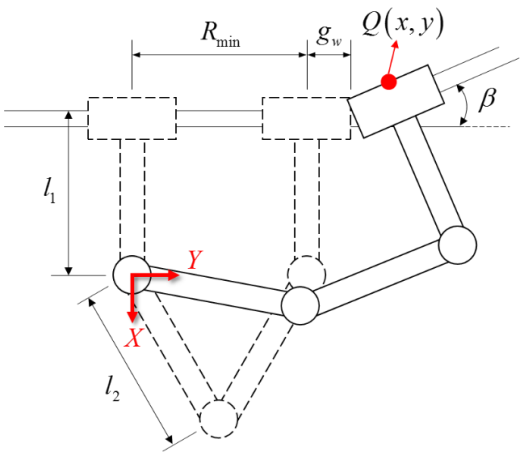

Fig. 4. The target grasping position $Q(x,y)$ for pitched ledge climbing.

Substituting the numerical values of the parameters l_1, l_2, R_{min}, and g_w allows us to find the maximum pitched ledge angle the robot can climb. For example, the simulation results shown in Fig. 5 indicate that the designed robot can overcome the ledge transition with a pitched angle up to 41°, i.e., $\beta \le 41°$.

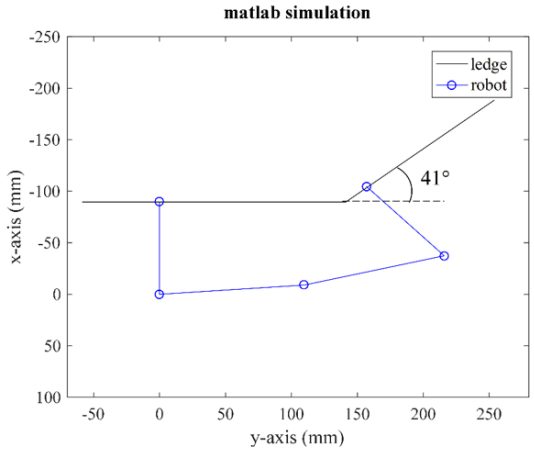

Fig. 5. Kinematic constraint for multi-step crossing: the ledge pitched angle must be within the range between 41° and -41°.

2) Detection and Estimation of Pitched Angle

To explain how the robot detects the existence of pitched ledge and measures the pitched angle using infrared sensors, a sensor placement configuration is defined as Fig. 6. *Ds* is the distance between the sensor and the ledge. θ_{su} is the angle between the radiating light of the upper sensor and the vertical axis. h_{su} is the vertical distance between the radiating point of the upper sensor and the ledge. g_{su} is the offset distance for the adjustment of the upper sensor. Similarly, θ_{sd} is the angle between the radiating light of the lower sensor and the vertical axis. h_{sd} is the vertical distance between the radiating point of the lower sensor and the ledge. g_{sd} is the offset distance for the adjustment of the lower sensor. g_h is the reserved space for the gripper movement. s_h and s_w represent the height and width of the IR sensor, respectively. As shown, one sensor looking down is used to measure the distance variation for the case of climbing up (positive pitched angles), while the other sensor looking up is used to measure the distance variation for the case of climbing down. In this study, the parameters of the sensor configuration are listed as Table I.

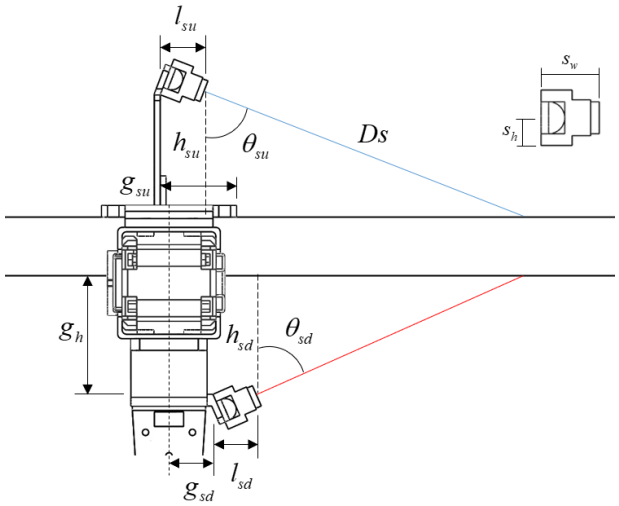

Fig. 6. Placement of two infrared sensors in one robot arm.

TABLE I. PARAMETERS SHOWN IN FIG. 6.

Upper infrared sensor (looking down)		Lower infrared sensor (looking up)	
g_{su}	26 mm	g_{sd}	15 mm
h_{su}	43.2 mm	h_{sd}	41 mm
θ_{su}	68.9^0	θ_{sd}	66.3^0

When the robot is climbing along a horizontal ledge, the sensor reading values *Ds* are almost the same, i.e., the variation of *Ds* is minimal. However, the value of *Ds* starts to change when the sensor detects a slope variation along the climbing ledge. Fig. 7 shows the relationship between two consecutive measurements in the presence of a ledge pitched angle β. ds_1 is the measured value the sensor initially detects a difference from previous reading values. ds_2 is the next measured value after the gripper moves right to a certain distance *b*, which can be calculated by using the motor encoder readings. θ_{su} is the angle between the radiating light of the infrared sensor and the vertical axis. Using the fact that $a = ds_1 - ds_2$ and the law of cosines for the zoomed in triangle ABC twice, one can obtain the length *c* and the ledge pitched angle β as

$$c = \sqrt{a^2 + b^2 - 2ab\cos(90° - \theta_s)}$$
$$\beta = \angle A = \cos^{-1}\left(\frac{b^2 + c^2 - a^2}{2bc}\right) \quad (6)$$

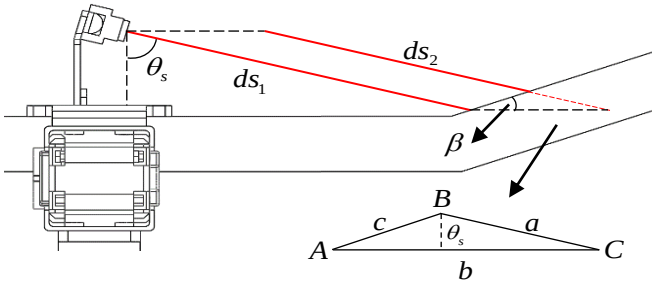

Fig. 7. Measured parameters in the presence of a ledge pitched angle β.

III. LOCOMOTION CONTROL FOR HORIZONTAL AND PITCHED LEDGE CLIMBING

In this study, locomotion control strategies are developed for climbing horizontal and pitched ledges, which are commonly seen in outdoor building scenarios. For horizontal ledge climbing the locomotion seems to be repetitive and rhythmic according to the locomotion represented in the video of extreme athletes. This locomotion could be simply implemented via the concept of inverse kinematics and path planning for most climbing robots. However, when the ledges the robot is climbing include variations such as pitched ledges, it is a non-trivial task that the robot can detect the existence of pitched ledges in advance and adjust its locomotive behavior to overcome the transition between ledges with unknown pitched angles. This study proposes using several central pattern generators to generate the rhythmic climbing behaviors for horizontal climbing [1] and develop a novel locomotion control strategy integrating with a number of infrared sensors to deal with the problem of pitched ledge detection and path planning.

A. Locomotion Control Strategy

Before introducing the proposed locomotion control strategy we briefly review the applied CPG control strategy based on a Kuramoto model [18], which can be represented as follows:

$$\dot{\phi}_i = \omega_i + \sum_j [\omega_{ij} r_j \sin(\phi_j - \phi_i - \varphi_{ij})]$$
$$\ddot{r}_i = a_r\left(\frac{a_r}{4}(R_i - r_i) - \dot{r}_i\right)$$
$$\ddot{x}_i = a_x\left(\frac{a_x}{4}(X_i - x_i) - \dot{x}_i\right) \quad (7)$$
$$\theta_i = x_i + r_i \sin(\phi_i)$$

where θ_i is the oscillating set-point; ϕ_i, r_i, x_i are the state variables of the phase, amplitude, and offset of the oscillators, respectively; ω_i, R_i, X_i are the parameters affecting the frequency, amplitude, and offset of the oscillators; w_{ij} and φ_{ij} are the coupling weights and the parameters that determine the phase of the i^{th} oscillator influenced by the j^{th} oscillator; a_r and a_x are the constant variables.

Suppose that the robot starts the climbing motion with a horizontal ledge followed by slope change along the incoming path. Note that only continuous ledges are considered in this study. As shown in Fig. 8, the robot is supposed to perform continuous ledge climbing locomotion using the designed CPG algorithm. The details of finding proper design parameters for the CPG algorithm and experiments of horizontal ledge climbing can be referred to [1]. When the robot detects any ledge slope change during the climbing process, the locomotion control will be switched from CPG control to a path planning strategy that obtains a proper gripper grasping position on the pitched ledge and calculates the motor commands for desired locomotion control. The kinematic constraint used to determine whether the robot passes through the inclined transition is that summation of the joint angles of the robot body must be 180° while hanging on a horizontal ledge. This constraint can be represented as

$$\theta_1 + \theta_2 + \theta_3 = 180° \quad (8)$$

where θ_1, θ_2, θ_3 are the joint angles for *Al*, *Am*, *Ar* shown in Fig. 2, respectively. The robot recognizes the finish of passing

through the inclined transition and returns to the posture for continuous horizontal ledge climbing once this kinematic constraint is satisfied.

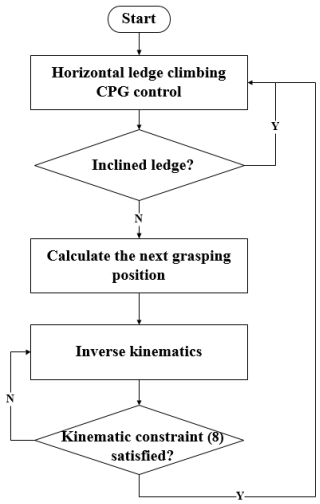

Fig. 8. Flow chart of the locomotion control strategy used for the developed ledge climbing robot.

1) Gripper posture compensation

One assumption made in the proposed locomotion control strategy and analysis is that the grasped gripper maintains a posture such that the ledge holding arm is perpendicular to the ledge. Because the parameter values of the sensor configuration (shown in Fig. 6) are selected based on this assumption, violation of this assumption may deteriorate the measurement sensitivity of the IR sensors, and even more seriously, the effectiveness of the estimated pitched angle for locomotion control. Taking an example of climbing right, Fig. 9 shows this constraint with a gripper posture angle θ_g which must be 90°. The coordinates of joints *Ar* and *Gr* are represented as (x_{Ar},y_{Ar}) and (x_{Gr},y_{Gr}), which could be simply found by the encoder feedback values and forward kinematics. This angle can be expressed as

$$\theta_g = \tan^{-1}\left(\frac{x_{Gr} - x_{Ar}}{y_{Gr} - y_{Ar}}\right) \quad (9)$$

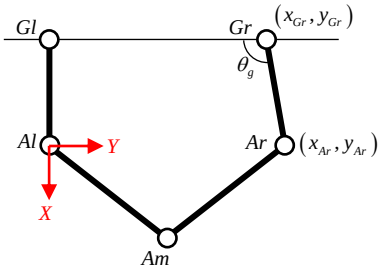

Fig. 9. Gripper posture constraint: θ_g must be 90°.

The effects of violating gripper posture constraint can be illustrated using the simulation results in the case of horizontal ledge climbing. Fig. 10 shows the variation of θ_g using CPG control. Clearly, there exists a constant deviation (≈ 2°) from the desired value 90° after transience. The reason affecting this posture error is due to the setting of parameters R_i and X_i in the oscillators. This is because the gripper posture is highly related to the pace affected by the amplitude of the oscillators (R_i) and the given motor commands affected by the setting points in the oscillators (X_i).

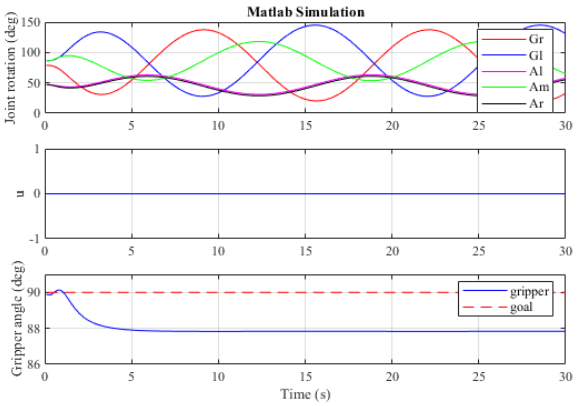

Fig. 10. Gripper posture during horizontal ledge climbing (without feedback control). Upper plot: robot joint motion; middle plot: offset of the oscillators X_i = 0; lower plot: gripper posture θ_g.

A feedback control system for regulating the grasping gripper posture is proposed to eliminate the steady state posture errors under continuous horizontal ledge climbing, as shown in Fig. 11. A PID (Proportional Integral Derivative) control law is adopted to adjust the parameters X_i of each oscillator online according to the current gripper posture, where the feedback term θ_g can be obtained using (9). The values of the PID control parameters are empirically chosen as K_p = 0.1, K_i = 0.25, K_d = 0.28. For simplicity the parameter R_i is fixed in this study. Fig. 12 shows the gripper posture compensation results after applying the proposed feedback control system, where the middle plot also indicates the calculated X_i. The simulation results show that the gripper posture error primarily occurs at the transience, such as starting the locomotion from rest or changing the climbing direction.

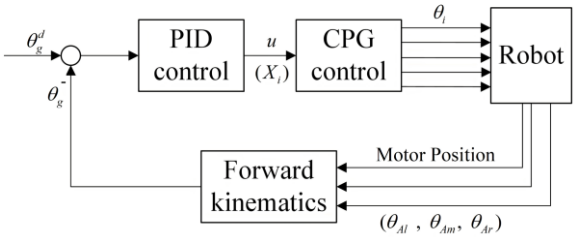

Fig. 11. Block diagram of gripper posture feedback control system.

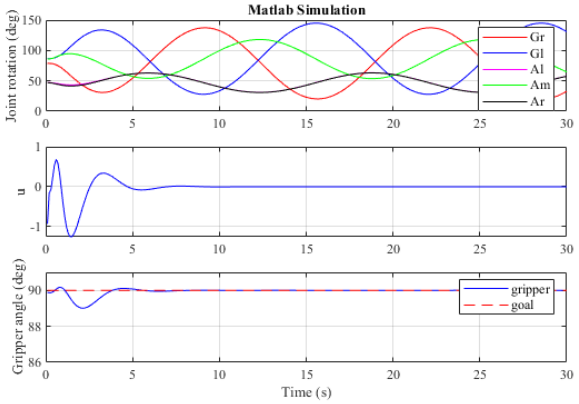

Fig. 12. Gripper posture compensation using feedback control. Upper plot: robot joint motion; middle plot: PID control input (X_i); lower plot: gripper posture θ_g.

2) Path planning of gripper grasping during inclined transition

As mentioned above, the robot will switch the locomotion control strategy to the path planning mode when detecting an environmental difference, i.e., horizontal ledge becomes pitched ledge or vice versa. During inclined transition the grasping positions for two grippers will be calculated using IR sensor feedback and motion control is implemented using robot inverse kinematics. Suppose that the IR reflection point on the measured position is (x_s,y_s). Fig. 13 shows the schematic diagram of ledge climbing with inclined transition, where the plots are made with the assumption of moving right for easier explanation. The goal here is to find the target grasping positions for two grippers such that the right hand can land on the pitched ledge and the left hand can move forward on the horizontal ledge synchronously.

To achieve this goal the first step is to find the reflection point (x_s,y_s) using geometric relationship of sensor setup and right gripper holding position (R_x,R_y). Using the coordinate system defined in the figure, one can derive the coordinate values of the reflection point as follows

$$\begin{cases} x_s = R_x - h_{su} + ds_u \cos\theta_{su} \\ y_s = R_y + \Delta + ds_u \sin\theta_{su} \end{cases} \tag{10}$$
$$\Delta = s_h \cos\theta_{su} + s_w \sin\theta_{su} - (g_{su} - g_w)$$

Here s_h and s_w represent the height and width of the IR sensor, and Δ is the horizontal distance between the center point of the right gripper and the radiating point. The values of R_x and R_y can be simply obtained using encoder feedback and kinematics.

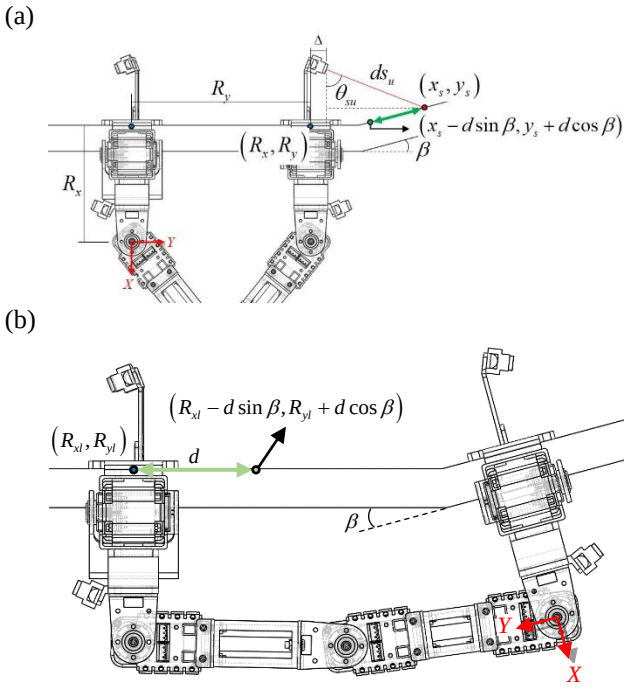

Fig. 13. Finding the grasping position during inclined transition. (a) right hand grasping position on the pitched ledge; (b) left hand grasping position on the horizontal ledge.

The next step is to find the maximum gripper moving distance based on the reflection point. Suppose the target position to be (x_{gr},y_{gr}) = $(x_s - d\sin\beta, y_s + d\cos\beta)$, where β is the pitched angle and d is the moving distance along the pitched ledge. The distance d is a variable which should satisfy the mechanism constraint and determines whether the target grasping position (x_{gr},y_{gr}) is on the right side or left side of the reflection point (x_s,y_s). The range and maximum value of d can be obtained using a similar analysis done in Section II.2.

After making a first move, the second move requires that the left gripper steps forward and reaches a posture with two hands as close as possible. Again, using the same analysis done above, one can obtain the target grasping position for the left gripper as

$$(x_{gl}, y_{gl}) = (R_{xl} - d\sin\beta, R_{yl} + d\cos\beta)$$

(R_{xl},R_{yl}) denotes the coordinate values of the left gripper obtained by kinematics. The process of calculating target grasping position and moving forward is repeatedly performed until the kinematic constraint (8) satisfies, meaning that the robot has successfully passed through the inclined transition and is ready for horizontal ledge climbing. Therefore, the locomotion control strategy is switched back to the CPG control mode while continuing detecting the existence of the ledge inclination ahead.

IV. Experiments and Discussion

In this section a set of experiments are first presented to analyze the effects of the detection range, ledge pitched angle, and success rate of slope detection. Ledge climbing experiments mimicking the cases of climbing along a double pitched roof and a single pitched roof are then conducted to evaluate the feasibility of the proposed locomotion control strategy.

A. Ledge Slope Detection

The principle of the ledge slope detection method uses the measurement of IR sensors and gripper position change to detect the existence of pitched ledge, in which the pitched angle can be estimated with a consecutive two-times sensor reading action. The first reading is recorded when the measured distance is significantly decreased than the previous sensor reading values. To maximize the measured range the second reading is recorded at the moment that the gripper makes the largest pace. The measured distance for the above action is averaged with twenty reading values while the largest and smallest five records are moved for better results.

In this study the moving distance of every locomotion cycle is fixed by using the same parameters in the CPG algorithm. It is obvious that the measured range varies with different starting robot position. In the following a set of experiments measuring the distance under different pitched angles and starting positions are performed to clarify this effect and the effectiveness of the used method. The effective estimation is defined such that the pitched angle error is within ± 5° because the robot is still able to perform desired climbing motion within this range after testing. Therefore, any deviation from the actual pitched angle beyond ± 5° is treated as a failed estimation.

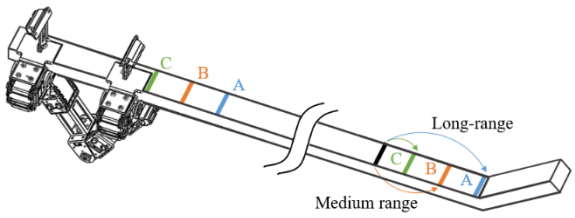

Fig. 14. Testing of pitched angle measurement.

Fig. 14 shows the setup of the testing scenarios for ledge slope detection, where the parameters affecting the estimation results include three pitched angles (10°, 20°, 30°) and three starting positions (A, B, C). The robot climbing pace is approximately 8 cm every locomotion cycle. The black line indicates the first sensor reading that identifies the slope change. The difference between each starting position is 2 cm. The position A is the position after slope detection from previous sensor reading and the measured range covers the distance from the black line to the blue line. As can be seen, starting with the position A may eventually lead to the largest measurement range among these three testing positions. Similarly, the robot starting with the position C will move to the position farthest from the turning point and only can measure the distance range from the black line to the green line for pitched angle estimation. As a result, the starting position B provides a medium measured range aside from the other two starting positions A and C. The slope estimation algorithm is tested by performing ledge climbing experiments with twenty times repeated measurements under three different pitched angles and three starting positions.

Fig. 15 summarizes the testing results showing the success rate of the ledge slope detection. It is clear that the success rate is affected by the gripper starting position while the results at position A and B are close to each other but better than the ones at position C. This is because the smaller measured range is easily affected by the sensor measurement errors. The estimation seems to be more effective when measuring smaller pitched angles. The reason that the success of measuring larger pitched angles decreases is due to the improper sampled data for long time use and the time delay in digital filtering of IR sensor data. Fig. 15 also indicates that the success rate of detecting 30° pitched angles at position C downgrades to 60%. It is suggested that the robot can adjust the robot moving pace online to deal with the ledges with larger pitched angles. This issue could be investigated further by formulating an optimization problem that searches a proper gripper starting position to ensure the correctness of the estimated slope values.

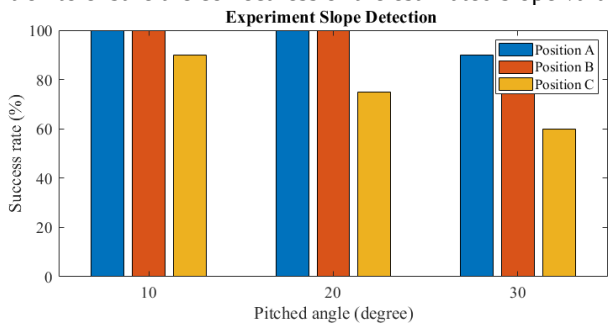

Fig. 15. Experiments: success rate of pitched ledge detection using the proposed method.

B. Ledge Climbing Experiments

Ledge climbing robots are designed to move along the ledges on the building walls, such as windowsills or eaves. In this work square Aluminum extrusions are used to set up the experiment test beds to evaluate the effectiveness of the proposed locomotion control strategy for pitched ledge climbing. Among the buildings with ledge structures, the roofs are the most commonly seen scenarios with pitched angles. The roofs of the buildings in general can be classified into three types according to the appearance: flat roof, pitched roof, and others. The drainage slope of the flat roofs is usually less than 5% so the horizontal ledge setup can be used to represent this experiment scenario. The pitched roofs, on the other hand, are the roofs with a drainage slope greater than 10%. Fig. 16 presents an example of doubled pitched roof in iron sheet houses which are very popular in Taiwan.

Fig. 16. Scene of a double pitched roof in iron sheet houses.

As mentioned in Section II, the maximum allowed pitch angle for robot to climb without violating the mechanism constraint is 41°. However, the hardware spec that the minimum measurement distance of the used IR sensor is 4 cm also imposes a constraint to reduce the success rate of detecting correct pitch angles. Considering this constraint together and performing a similar analysis done in Section II suggests that the maximum measured pitch angle using the lower infrared sensor (looking up or positive pitch angle) reduces to 30°, in which its slope is equal to tan(30°) ≈ 57.7%. In the following two sets of pitched ledge climbing experiments are conducted to mimic the scenarios of climbing along a double pitched roof (downward inclination) and a single pitched roof (upward inclination).

1) Scenario of ledge climbing along a double pitched roof (downward inclination)

Climbing along a double pitched roof is equivalent to climbing along a horizontal ledge first and then passing through a turning point with downward inclination. Fig. 17 shows the snap shots of ledge climbing experiments used to mimic the scenarios of climbing along a double pitched roof with a slope close to -57.7% (-30° pitch angle). The negative sign means the robot moves downward with respect to the turning point. The robot is supposed to perform horizontal ledge climbing using the CPG algorithm before detecting a pitched angle change. For conciseness the results of horizontal ledge climbing are omitted in the current study but can be found in our previous work [1].

As shown in the first subplot of Fig. 17 (t = 0 s), once detecting the ledge slope change the robot adjusts its posture such that the two hands are closest to each other and passes through the ridge using the path planning method presented in Section III, shown in the second and third subplots of Fig. 17 (t = 1.5 s and t = 8.47 s). After two hands are all at the same side, the robot then switches the locomotion control strategy back to the CPG algorithm for horizontal ledge climbing, as shown in the last subplot of Fig. 17 (t = 21.6 s). Fig. 18 presents the

experimental results for robot to perform a task of climbing from left to right (0 s ~ 43 s) and returning back from right to left (43 s ~ 77.5 s). A vertical dashed line at 43 s is made in each subplot to distinguish between these two routes. As can be seen, there exists an obvious time region that the robot switches the locomotion control strategy from CPG algorithm to path planning mode to overcome the ledge slope transition. The joint motion at these time regions is not as periodic as the one at other time regions, which makes sense because the robot is designed to find a feasible posture to overcome the inclined transition no matter what the robot starts with which gripper grasping position. Note that there always exists a truncation in robot joints *Gl* and *Gr* because of the limited gripping range for a rigid ledge.

There are four IR sensor reading values used to determine the ledge pitch angle ahead. The subscripts *ur*, *lr*, *ul*, *ll* in the plot denote the upper right, lower right, upper left, and lower left, respectively. Because the pitch angle of the double pitched roof is negative, only the measurements of the IR sensors placed below the grippers (ds_{lr} & ds_{ll}) are effective in calculating the pitched angle. In this scenario, the lower sensor at the right arm is valid for right ledge climbing and the lower sensor at the left arm is valid for left ledge climbing. It is found from the figure that the robot recognizes significant changes of pitched angle β at 18.4 s (climbing right) and 52.7 s (climbing left). The robot then switches to the path planning mode after approximately two seconds. The robot stops estimating β when passing through the inclined region because the estimation is made based on the two consecutive sensor measurements on the continuous ledge surface. Therefore, after successfully climbing over the ridge the robot resumes the pitch angle estimation and switches back to the CPG algorithm for horizontal ledge climbing. Although there are a few deviations of the estimated pitched angles (β_{lr} = 28.8° and β_{ll} = 32.9°) compared with the nominal value of 30°, the robot still performs the desired locomotion very well.

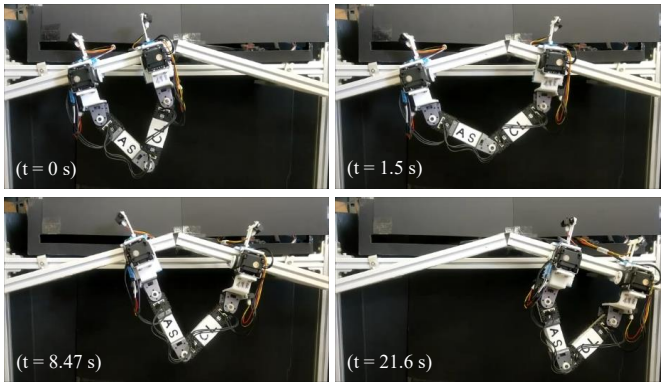

Fig. 17. Snap shots of ledge climbing experiments: mimicking the scenario of climbing along a double pitched roof with a negative pitched angle.

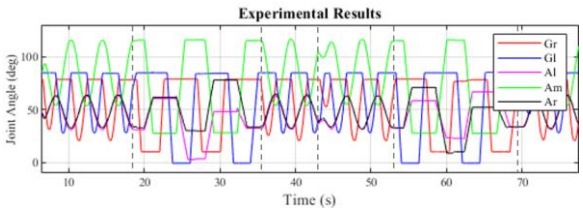

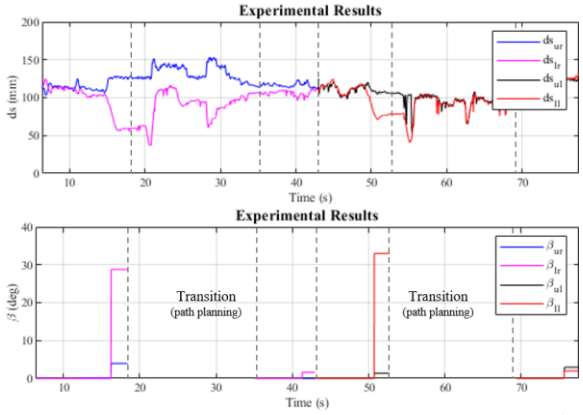

Fig. 18. Experimental results: climbing along a double pitched roof with a pitched angle of -30°. The upper plot: robot joint motion; the middle plot: measurement results of IR sensors; bottom plot: pitched angle information.

2) Scenario of ledge climbing along a single pitched roof (upward inclination)

Besides double pitched roofs, single pitched roofs are also very common in the neighboring buildings. The difference between these two kinds of roofs is that the pitch angles of double pitched roofs are always negative, while the pitch angles of single pitched roofs could be either positive or negative, depending on the inclination direction. This section specifically presents the results of ledge climbing with upward inclination to mimic the scenario of climbing along a single pitched roof. In this case, the robot always looks up to detect the environment change whenever encountering with a ledge slope.

Fig. 19 shows the snap shots of ledge climbing experiments used to mimic the scenarios of climbing along a single pitched roof with a slope close to 57.7% (30° pitched angle). The movement procedure is identical to the one in the previous experiments by letting the robot climb from left to right and return back. The experimental results of robot joint motion, IR sensor measurement, and estimated pitched angle are shown in Fig. 20. The results indicate that the robot takes a longer time during the path planning mode, which is about 6 s slower than the case with a -30° negative pitch angle. Therefore, the total climbing time for the assigned route is longer. The robot posture during ledge inclination is also different and more aggressive as shown in the snap shots. This is because the lower IR sensors used to detect the positive ledge slope are configured with more restrict mechanism constraints. One feasible strategy for solving this issue is to speed up the robot moving pace during CPG control mode and slow down the movement while passing through the inclined transition for safety reason. The video clips of the above conducted ledge climbing experiments can be found at the following web link: https://reurl.cc/Wk8x39.

V. CONCLUSION

This paper presents a locomotion control strategy for ledge climbing robots to implement pitched ledge climbing using CPG control and infrared sensors. The CPG algorithm is applied as the principal locomotion controller for horizontal ledge climbing. An environment detection algorithm is developed to determine the timing of switching to the path planning mode where the value of pitched angle is estimated to produce joint commands for robot to smoothly pass through the inclined transition. The experimental results indicate that the

proposed locomotion control strategy is feasible for back-and-forth ledge climbing and the robot is able to transversely move along the ledges with ± 30° pitched angles. Future work includes the analysis and improvement of robot moving pace and extension of advanced locomotion control to the application scenarios with non-uniform gaps along the climbing ledges. Motion planning without the use of infrared sensors is also an interesting research direction which is helpful to make the developed ledge climbing robot more practical.

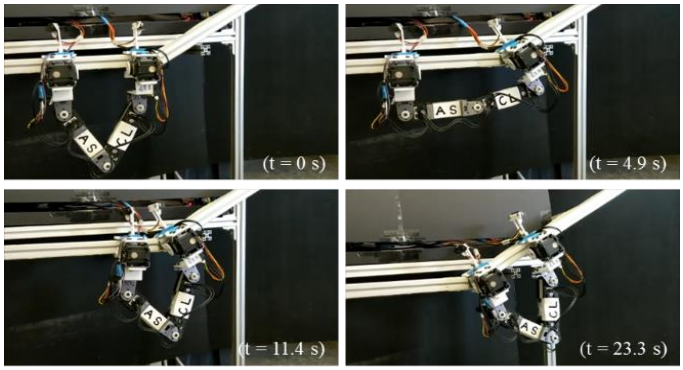

Fig. 19. Snap shots of ledge climbing experiments: mimicking the scenario of climbing along a single pitched roof with a positive pitched angle.

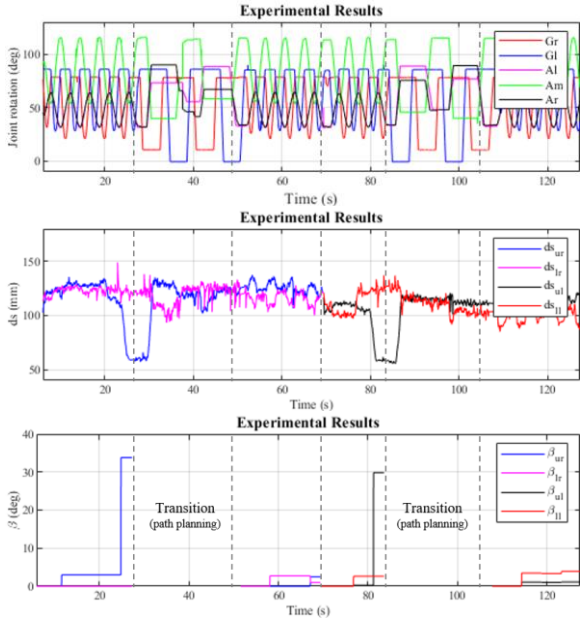

Fig. 20. Experimental results: climbing along a single pitched roof with a pitched angle of 30°. The upper plot: robot joint motion; the middle plot: measurement results of IR sensors; bottom plot: pitched angle information.

APPENDIX: NOMENCLATURE LIST

Symbol	Referred to
β	Ledge pitched angle
$R_{\min}$	Minimum distance between two holding hands
g_w	Half distance of the gripper width
D_S	Distance between sensor and ledge
θ_{su}	Angle between the radiating light of the upper sensor and the vertical axis
h_{su}	Vertical distance between the radiating point of the upper sensor and the ledge
g_{su}	Offset distance for upper sensor
θ_{sd}	Angle between the radiating light of the lower sensor and the vertical axis
h_{sd}	Vertical distance between the radiating point of the lower sensor and the ledge
g_{sd}	Offset distance for lower sensor
g_h	Reserved space for gripper movement
θ_i	CPG oscillator: oscillating set-point
φ_i	CPG oscillator: state variable of phase
r_i	CPG oscillator: state variable of amplitude
x_i	CPG oscillator: state variable of offset of the oscillators
w_i	CPG oscillator: parameters affecting the frequency
R_i	CPG oscillator: parameters affecting the amplitude
X_i	CPG oscillator: parameters affecting the offset of the oscillators
w_{ii} φ_{ii}	CPG oscillator: coupling weights and parameters that determine the phase of the i^{th} oscillator influenced by the j^{th} oscillator
a_r a_x	CPG oscillator: constant variables.
θ_g	Gripper posture angle
s_h	Height of the IR sensor
s_w	Width of the IR sensor
Δ	Horizontal distance between the center point of the right gripper and the radiating point

REFERENCES

[1] C.-Y. Lin and T.-C. Hu, "Development and locomotion control of a horizontal ledge-climbing robot," in *Proc. IEEE ICCAR*, Singapore, 2021. https://reurl.cc/X42Wle

[2] M. F. Silva and J. A. T. Machado, "A survey of technologies and applications for climbing robots locomotion and adhesion," in *Climbing and Walking Robots*. London, United Kingdom: IntechOpen, 2010 [Online]. https://www.intechopen.com/chapters/10079

[3] Y. Guan *et al.*, "A modular biped wall-climbing robot with high mobility and manipulating function," *IEEE/ASME Trans. Mechatron.*, vol. 18, no. 6, pp. 17871798, Dec. 2013. https://reurl.cc/Qj2949

[4] H. Zhu *et al.*, "Transition analysis and its application to global path determination for a biped climbing robot," *Appl. Sci.*, vol. 8, no.1, 122, Jan. 2018. https://www.mdpi.com/2076-3417/8/1/122/htm

[5] F. Saito, T. Fukuda, and F. Arai, "Swing and locomotion control for a two-link brachiation robot," *IEEE Control Syst. Mag.*, vol. 4, no. 1, pp. 5-12, Feb. 1994. https://ieeexplore.ieee.org/document/257888

[6] H. Kajima *et al.*, "A study on a brachiation controller for a multi-locomotion robot - realization of smooth, continuous brachiation," *Adv. Robot.*, vol. 18, no. 10, pp. 1025-1038, 2004. https://sci-hub.hkvisa.net/10.1163/1568553042674671

[7] Z. Luo *et al.*, "Swing control for a three-link brachiation robot based on sliding-mode control on irregularly distributed bars," *Mech. Sci.*, vol. 12, no. 2, pp. 1073-1081, 2021. https://ms.copernicus.org/articles/12/1073/2021/

[8] S. Farzan *et al*., "Feedback motion planning and control of brachiating robots traversing flexible cables," in *Proc. ACC*, Philadelphia, PA, USA, 2019. https://ieeexplore.ieee.org/document/8814894

[9] C.-Y. Lin and Z.-H. Yang, "TRBR: flight body posture compensation for transverse ricochetal brachiation robot," *Mechatronics*, vol. 65, 102307, Feb. 2020. https://www.sciencedirect.com/science/article/pii/S0957415819301394

[10] S. Nansai and R. E. Mohan, "A survey of wall climbing robots: recent advances and challenges," *Robot.*, vol. 5, no. 3, 14, 2016.

https://www.mdpi.com/2218-6581/5/3/14
[11] D. Longo and G. Muscato, "The Alicia3 climbing robot: a three-module robot for automatic wall inspection," *IEEE Robot. Autom. Mag.*, vol. 13, no. 1, pp. 42-50, Mar. 2006.
https://ieeexplore.ieee.org/document/1598052
[12] J. Shen and Y. Liu, "Design and analysis of an obstacle-crossing wall-climbing robot mechanism," in *Proc. IEEE CYBER*, Shenyang, China, 2015.
https://ieeexplore.ieee.org/document/7288267
[13] Y. Liu and T. Seo, "AnyClimb-II: dry-adhesive linkage-type climbing robot for uneven vertical surfaces," *Mech. Mach. Theory*, vol. 124, pp. 197-210, Jun. 2018.
https://www.sciencedirect.com/science/article/pii/S0094114X17310571
[14] H.-Y. Wu, "The research of roof drainage capacity influenced by rainfall intensity," M. S. thesis, Dept. Archit., China Univ. Tech., Taipei, Taiwan, 2013.
[15] A. Kamimura, H. Kurokawa, and E. Yoshida, "Automatic locomotion design and experiments for a modular robotic system," *IEEE/ASME Trans. Mechatron.*, vol. 10, no. 3, pp. 314-325, Jun. 2005.
https://ieeexplore.ieee.org/document/1461408
[16] J. Yu *et al.*, "A survey on CPG-inspired control models and system implementation," *IEEE Trans. Neural Netw. Learn. Syst.*, vol. 25, no. 3, pp. 441-456, Mar. 2014.
https://ieeexplore.ieee.org/document/6605609
[17] T. Kang, H. Kim, and H. Choi, "Realtime perception with infrared scanner for navigation of quadruped walking and climbing robot," in *Proc. IEEE/RSJ IROS*, Japan, 2004.
https://ieeexplore.ieee.org/document/1389792
[18] J. A. Acebrón *et al.*, "The Kuramoto model: a simple paradigm for synchronization phenomena," *Rev. Mod. Phys.*, vol. 77, no. 1, pp. 137–185, 2005.
https://journals.aps.org/rmp/abstract/10.1103/RevModPhys.77.137

Chi-Ying Lin Chi-Ying Lin received the B.S. and M.S. degrees from National Taiwan University, Taiwan in 1999 and 2001, respectively, and the Ph.D. degree from University of California, Los Angeles in 2008, all in mechanical Engineering. He is currently a full Professor in the Department of Mechanical Engineering at National Taiwan University of Science and Technology, Taiwan. His recent research interests include (1) design, modeling, and locomotion control of bio-inspired brachiating robots; (2) active vibration control of smart flexible structures using piezoelectric electrode configuration techniques; and (3) development of novel robotic systems integrated with the techniques of visual servoing and force feedback.

Ting-Chun Hu received B.S. degree in 2016 from National Taipei University of Technology, Taiwan and M.S. degree in 2018 from National Taiwan University of Science and Technology, Taiwan, all in mechanical engineering. Her research interests include bio-inspired climbing robots and locomotion control.